Cerebellum (2015) 14:106–118
DOI 10.1007/s12311-014-0618-8

ORIGINAL PAPER

Compartmentation of the Cerebellar Cortex: Adaptation to Lifestyle in the Star-Nosed Mole *Condylura cristata*

Hassan Marzban · Nathan Hoy · Matthew Buchok · Kenneth C. Catania · Richard Hawkes

Published online: 22 October 2014

Abstract The adult mammalian cerebellum is histologically uniform. However, concealed beneath the simple laminar architecture, it is organized rostrocaudally and mediolaterally into complex arrays of transverse zones and parasagittal stripes that is both highly reproducible between individuals and generally conserved across mammals and birds. Beyond this conservation, the general architecture appears to be adapted to the animal's way of life. To test this hypothesis, we have examined cerebellar compartmentation in the talpid star-nosed mole *Condylura cristata*. The star-nosed mole leads a subterranean life. It is largely blind and instead uses an array of fleshy appendages (the "star") to navigate and locate its prey. The hypothesis suggests that cerebellar architecture would be modified to reduce regions receiving visual input and expand those that receive trigeminal afferents from the star. Zebrin II and phospholipase Cß4 (PLCß4) immunocytochemistry was used to map the zone-and-stripe architecture of the cerebellum of the adult star-nosed mole. The general zone-and-stripe architecture characteristic of all mammals is present in the star-nosed mole. In the vermis, the four typical transverse zones are present, two with alternating zebrin II/PLCß4 stripes, two wholly zebrin II+/PLCß4−. However, the central and nodular zones (prominent visual receiving areas) are proportionally reduced in size and conversely, the trigeminal-receiving areas (the posterior zone of the vermis and crus I/II of the hemispheres) are uncharacteristically large. We therefore conclude that cerebellar architecture is generally conserved across the Mammalia but adapted to the specific lifestyle of the species.

Keywords Cerebellum · Cerebellar adaptation · Purkinje cell · Stripes

H. Marzban (✉) · M. Buchok
Department of Human Anatomy and Cell Science, Manitoba Institute of Child Health (MICH), College of Medicine, Faculty of Health Sciences, University of Manitoba, Rm129, BMSB, 745 Bannatyne Avenue, Winnipeg, Manitoba R3E 0 J9, Canada
e-mail: Hassan.Marzban@med.umanitoba.ca

N. Hoy · R. Hawkes
Department of Cell Biology and Anatomy, Hotchkiss Brain Institute, and Genes and Development Research Group, Cumming School of Medicine, University of Calgary, Calgary, Alberta T2N 4 N1, Canada

K. C. Catania
Department of Biological Sciences, Vanderbilt University, Nashville, TN, USA

Introduction

The adult mammalian cerebellum is histologically uniform. However, concealed beneath the simple laminar architecture, it is organized rostrocaudally and mediolaterally into reproducible arrays of transverse zones and parasagittal stripes [1–6]. The most extensively studied zone and stripe marker is the antigen zebrin II ([7]; reviewed in [2, 3, 5, 8]: the respiratory isoenzyme aldolase C [9, 10]). Zebrin II is expressed by a subset of Purkinje cells that forms a symmetrical array of parasagittal stripes (zebrin II+) that alternate with a subset of Purkinje cells that do not express zebrin II. The zebrin II-immunonegative (zebrin II−) Purkinje cells can be positively identified by the selective expression of other compartmentation markers such as phospholipase Cß4 (PLCß4; [11, 12]). Zebrin II+ stripes are numbered from P1+ medially to P7+ laterally: zebrin II− stripes (P−; all PLCß4+) are numbered according to the immediately medial P+ stripe [13, 14]. The Purkinje cell stripes align with the terminal fields of both mossy fibers (e.g., [15–18]) and climbing fibers (e.g., [19–21]); functional mapping studies have revealed a correlation between receptive field boundaries and zebrin stripes [22–24]; and several recent reports describe functional differences between Purkinje cell subsets [25–30].

The Purkinje cell stripes of zebrin II/PLCß4 expression are grouped into distinct transverse zones. The mouse cerebellum is subdivided into five transverse zones. The boundaries between zones are typically not abrupt but rather interdigitate extensively. The anterior zone (AZ) occupies lobules I–V of the vermis, extending caudally into the primary fissure. Lobules VI–VII constitute the central zone (CZ), which is further divided into an anterior component (CZa: ~lobule VI) and a posterior component (CZp: lobule VII; [31]). The posterior zone (PZ) comprises lobule VIII and dorsal lobule IX. Finally, the nodular zone (NZ) consists of ventral lobule IX and lobule X [4, 32]. In birds, an additional zone, the lingular zone (LZ), occupies lobule I [33–35]. The AZ and PZ consist of alternating zebrin II+ and PLCß4+ stripes; Purkinje cells in the CZ and NZ (and LZ) are uniformly zebrin II+/PLCß4−. There is no fixed relationship between lobule boundaries and transverse zones—the precise alignment varies between species (e.g., the CZ occupies all lobules VI/VII in mouse but is restricted to lobule VI in the naked mole-rat [36] and some mutations seem to alter the two independently (e.g., *cerebellar deficient folia* [37]).

The zone-and-stripe architecture of the cerebellar cortex is both highly reproducible between individuals (e.g., [7]) and well conserved across mammals and birds (e.g., [38, 39]). Zebrin II+ Purkinje cells are also found in fish (e.g., [7, 40]) and reptiles [38]. Despite the high level of conservation, species-specific adaptations are also apparent. For example in the naked mole-rat, which is functionally blind, the visual-receiving CZ is unusually small [36]. Conversely, in bats, the CZ is unusually elaborate, perhaps to subserve the needs of echolocation [41].

Two distinct theories describe the way brains vary in size between species. In one case, evolutionary selection for enlargement of any one brain part is constrained to the enlargement of the whole brain (e.g., [42]). Alternatively, different brain parts, or functionally coupled neural systems, may change independently—mosaic rather than concerted evolution (e.g., [43]). In the cerebellum, this implies either that when one region expands to meet a functional need, all the rest do as well, or that the cerebellum comprises a mosaic of multiple systems that can expand or contract independently. To begin to test the hypothesis that cerebellar architecture is a highly conserved mosaic that adapts to specific lifestyles, we have examined cerebellar compartmentation in the star-nosed mole *Condylura cristata*, a hamster-sized talpid (family *Talpidae*—the moles) found in wet lowland areas of eastern Canada and the northeastern USA. *Condylura* leads a subterranean and semi-aquatic life and is functionally blind. Its prey is located by using an array of mobile, fleshy appendages ("the star") at the end of the snout [44], a mechanosensory adaptation of the trigeminal system (e.g., [44, 45]). Given its unusual lifestyle, *Condylura* is predicted by the mosaic model to show two specific adaptations in its cerebellar architecture: first, a reduction in visual areas, and secondly, an expansion of those parts of the cerebellum receiving trigeminal inputs. Zebrin II and PLCß4 immunocytochemistry was used to map the zone-and-stripe architecture of the cerebellum of the adult star-nosed mole. Consistent with the hypothesis, the data revealed a strikingly small central zone of the vermis (visual) accompanied by an unusually large posterior zone and crus I/II of the hemispheres (trigeminal). We therefore conclude that cerebellar architecture behaves as a mosaic to adapt to specific evolutionary pressures.

Materials and Methods

Animals

All animal procedures conformed to institutional regulations and the Guide of the Care and Use of Experimental Animals from the Canadian Council of Animal Care. Adult star-nosed moles *C. cristata* (N=14, both males and females) were obtained from Vanderbilt University after being collected in Pennsylvania under permit no. COL00087 (for details, see [46]). Animals selected for the study were of different sizes and weights (typical adult individuals are 15–20 cm long and weigh about 55 g; no systematic interindividual differences were found although the immunostaining tended to be less consistent than in mice).

Adult *C. cristata* (>35 days) were deeply anaesthetized with sodium pentobarbital (120 mg/kg, i.p.) and transcardially perfused with 0.9 % NaCl in 0.1 M phosphate buffer (pH 7.4) followed by 4 % paraformaldehyde in 0.1 M phosphate buffer (pH 7.4). The brains were then removed, post-fixed in the same fixative at 4 °C for several days, and stored in buffer.

Antibody Characterization

The following antibodies were used:

1. Anti-zebrin II: Cerebellum of the star-nosed mole is a mouse monoclonal antibody produced by immunization with a crude cerebellar homogenate from the weakly electric fish *Apteronotus* [7] and subsequently shown to bind the respiratory isoenzyme aldolase C (Aldoc; [9, 10]), and it was used directly from spent hybridoma culture medium diluted 1:400. On immunoblots, anti-zebrin II recognizes a single polypeptide band, apparent molecular weight 36 kDa, in species from fish to mammals (e.g., [38]). In cerebellum, zebrin II immunoreactivity is restricted to a subset of Purkinje cells (e.g., [7]), with possible weak expression in glia [47].
2. Anti-phospholipase Cß4: Rabbit anti-phospholipase Cß4 (anti-PLCß4) was raised against a synthetic peptide representing amino acids 15–74 of the mouse PLCß4 protein fused to glutathione-*S*-transferase and expressed in bacteria (used diluted 1:1,000). Control immunohistochemistry by using either antibody preabsorbed with

antigen polypeptides or cerebellar sections from a PLCß4 knockout mouse yielded no significant immunostaining [11, 12]. Anti-PLCß4 recognizes a single polypeptide band of 134 kDa apparent molecular weight on Western blots of mouse [48] and human (unpublished data) cerebellar homogenates. The band is absent from Western blots of cerebellar homogenates from a PLCß4 null mouse [48]. In the mouse cerebellum, PLCß4 is expressed in the zebrin II-immunonegative subset of Purkinje cells [11, 12].

3. Anti-calbindin: Two different anti-calbindin antibodies were used. Rabbit anti-calbindin D-28K antiserum (anti-CaBP, diluted 1:1,000) was produced against recombinant rat calbindin D-28K. On immunoblots, it recognizes a single band of apparent molecular weight 27–28 kDa (manufacturer's datasheet, Swant Inc., Bellinzona, Switzerland, code no. CB38). Mouse monoclonal anti-calbindin (diluted 1:1,000) raised against chicken calbindin, specifically stains the ^{45}Ca-binding spot of calbindin D-28K (apparent molecular weight 28 kDa, isoelectric point 4.8) in a two-dimensional gel of mouse brain homogenate (manufacturer's information, Swant Inc., Bellinzona, Switzerland, code no. 300). Both anti-calbindin antibodies yielded identical Purkinje cell specific immunostaining that was completely consistent with that reported often before [4, 49, 50].

Immunocytochemistry

Peroxidase immunohistochemistry was carried out on free-floating sections as described previously [51]. Briefly, tissue sections were washed thoroughly, blocked with 10 % normal goat serum (Jackson Immunoresearch Laboratories, West Grove, PA) and then incubated in 0.1 M phosphate-buffered saline (PBS) buffer containing 0.1 % Triton-X100 and 5 % bovine serum albumin (blocking solution) and the primary antibody for 16–18 h at room temperature. Finally, sections were incubated in biotinylated goat anti-rabbit or biotinylated goat anti-mouse Ig antibody (diluted 1:1,000 in blocking solution; Jackson Immunoresearch Laboratories, West Grove, PA) for 2 h at room temperature, and binding revealed by using diaminobenzidine (Vectastain ABC Staining Kit, Vector Laboratories Inc., Burlingame, CA). Sections were mounted on slides, dehydrated through an alcohol series, cleared in xylene, and cover-slipped with Entellan mounting medium (BDH Chemicals, Toronto, ON).

Cerebellar sections for fluorescent immunohistochemistry [51] were washed, blocked in PBS containing 10 % normal goat serum (Jackson Immunoresearch Laboratories, West Grove, PA), and incubated in blocking solution containing the primary antibody for 16–18 h at 4 °C. Following incubation in primary antibodies, sections were washed and then left for 2 h at 4 °C in PBS containing CY3-conjugated goat anti-rabbit secondary antibody (Alexa conjugated Abs) and CY2-conjugated goat anti-mouse secondary antibody as appropriate (both diluted 1:1,000; Jackson Immunoresearch Laboratories, West Grove, PA). After incubation in secondary antibody, sections were washed in 0.1 M PBS buffer, mounted onto chrome-alum and gelatin subbed slides, air-dried overnight, cleared in xylene, and cover-slipped with non-fluorescing mounting medium (Fluorsave Reagent, Calbiochem, La Jolla, CA).

Photomicrographs were captured with a SPOT Cooled Color digital camera (Diagnostic Instruments Inc., Sterling Heights, MI) running under Adobe Photoshop 9. The images were cropped and corrected for brightness and contrast but not otherwise manipulated. The rostrocaudal length of the Purkinje cell layer was measured from sagittal sections through the vermis close to the midline. Images were captured and then measured by using Zen Pro 2012 software.

Results

Cerebellar Morphology

The external appearance of the cerebellum of *C. cristata* is shown from the dorsal aspect in Fig. 1a. There is a central vermis with large hemispheres on each side. An acortical area that lacks molecular and Purkinje cell layers is located in the paramedian sulcus between the vermal and hemispheric components of the CZ (white asterisks). A similar acortical area is found in several species (e.g., rat [52], rabbit [53], and bat [41]), but not all (e.g., the naked mole-rat [36]).

Cerebellar lobules are clearly distinguishable in sagittal sections through the vermis (Fig. 1b) and are labeled from rostral (lobule I) to caudal (lobule X). Lobules I to V, separated by well-developed fissures, can be delineated in the large anterior lobe of the vermis. The anterior lobe is separated from the posterior lobe by the primary fissure, which is prominent but capped by the anterior extension of lobule VI. Lobule VI is separated by the posterior superior fissure from the extensive lobules VIIa,b,c (Fig. 1a, b). Lobule VIII is small and seems to be compressed by the caudal extension of lobule VIIc and the rostral extension of lobule IXa, but the prepyramidal and secondary fissures are nonetheless evident (Fig. 1b). Finally, in the most caudal vermis, lobule IXb is separated from lobules Xa,b by the posterolateral fissure. In the hemispheres, the hemispheric extension of the posterior superior fissure separate lobulus simplex a,b from the lobulus ansiformis (subdivided into crus Ia,b and IIa,b by the intercrural fissure; Fig. 1a, white arrow). Caudally, the paramedian lobule is apparent (Fig. 1a). The small hemispheric component of

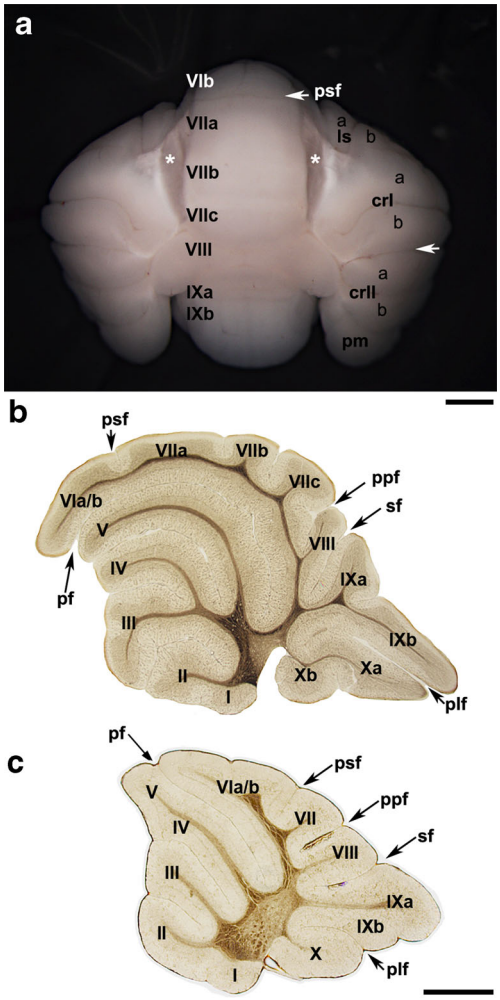

Fig. 1 The cerebellum of the adult star-nosed mole. **a** Low magnification image of the unstained cerebellum of the star-nosed mole, seen from dorsal. The vermis on each side is separated by the paramedian sulcus from the hemispheres. Acortical areas are indicated by *white asterisks*. **b** A sagittal section through the cerebellar vermis of the adult star-nosed mole. Lobules are indicated by *Roman numerals*. Lobules I–V are located anterior to the primary fissure (pf). Lobule VI is separated from the especially large lobule VII by the posterior superior fissure (psf). Lobule VII extends caudally to cover the prepyramidal fissure (ppf) that continues to the small lobule VIII. The secondary fissure (sf) is located between lobules VIII and IXa. Lobules IX and X are also prominent; prominent fissures and the medial nucleus are labeled. The rostrocaudal length of the vermis is ~54 mm. **c** A sagittal section through the cerebellar vermis of an adult mouse is shown for comparison. The rostrocaudal length of the vermis is ~30 mm. *crl* crus I, *crII* crus II, *ls* lobulus simplex, *pm* paramedian lobule, *psf* posterior superior fissure. *Scale bars*=1 mm (color figure online)

lobule VIII, the copula pyramidis, is concealed by the large caudal extension of crus II and the paramedian lobule.

Compartmentation Antigen Expression in the Cerebellum

Sections through the cerebellar cortex of the star-nosed mole immunoperoxidase stained with anti-zebrin II show a characteristic distribution of Purkinje cells. The reaction product is deposited in the somata, dendrites, and axons (Fig. 2a). No other cell types are stained. A similar restriction of immunoreactivity in the cerebellum has been reported from multiple species (e.g., [38, 39]). In some species, additional, weak immunoreactivity is seen in the somata of Bergmann glial cells (e.g., mouse [47]): this was not seen in the star-nosed mole. Not all Purkinje cells in the star-nosed mole express zebrin II. Rather, transverse sections through the vermis show consistently strong anti-zebrin II immunoreactivity in some Purkinje cells (black arrow) and weak or no staining of the rest (e.g., lobule V; Fig. 2b). The pattern of zebrin II expression is symmetrical about the midline and reveals an array of parasagittal stripes (Fig. 2c) reminiscent of those seen in many mammals, including rodents (e.g., mouse [14], rat [7], and hamster [54]) and bats [41].

In many species, PLCß4 is a positive antigenic marker of the zebrin II-immunonegative Purkinje cell subset. Purkinje cell somata and dendrites both express PLCß4 (Fig. 2d) in the star-nosed mole, but it is not detected in the Purkinje cell axons (this is also the case in other species, e.g., mouse [11]). PLCß4 is not expressed in all Purkinje cells. Rather, anti-PLCß4 reaction product is deposited in some while others are either weakly stained or not immunoreactive (Fig. 2e). The result is that anti-PLCß4 immunocytochemistry reveals an array of parasagittal stripes (Fig. 2f). Double immunostaining for CaBP and either zebrin II (Fig. 2g) or PLCß4 (Fig. 2h) confirms that the immunonegative stripes for zebrin II and PLCß4 are not due to the absence of Purkinje cells. Finally, double labeling for zebrin II and PLCß4 shows that the two Purkinje cell populations are non-overlapping (Fig. 2i) and comprise the entire Purkinje cell population.

Zone and Stripe Architecture

The expression patterns of zebrin II and PLCß4 in the star-nosed mole cerebellum reveal a complex, reproducible cytoarchitecture in the form of transverse zones and parasagittal stripes (Fig. 3).

AZ

The patterns of zebrin II (Fig. 4a) and PLCß4 (Fig. 4b) expression in the AZ resemble those reported in numerous other mammals (e.g., [11]). We have therefore adopted the usual stripe nomenclature here as well. A narrow P1+ stripe straddles the midline with P2+ to P4+ stripes on each side (seen both in immunoperoxidase (Fig. 4a) and immunofluorescence staining (Fig. 4c)). A second pair of zebrin II+ stripes (P2+) lies laterally on either side with their medial boundaries ~300 µm from the midline. A third pair (P3+) is located ~550 µm laterally from the

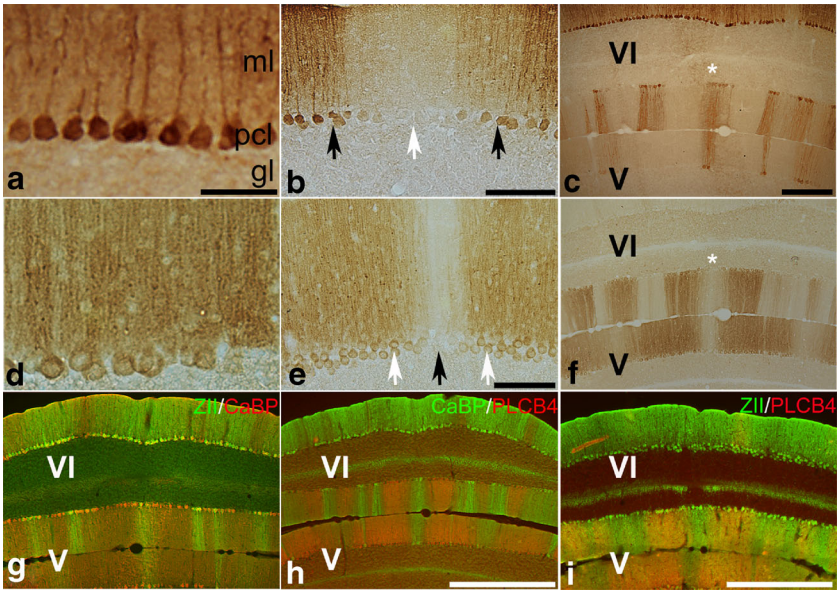

Fig. 2 Zebrin II and PLCß4 expression in the cerebellum of the star-nosed mole. **a** A transverse section through the cerebellum of the star-nosed mole immunoperoxidase stained by using anti-zebrin II. The Purkinje cell somata in the Purkinje cell layer (pcl) and dendrites in the molecular layer (ml) are strongly immunoreactive. **b** Immunoperoxidase staining for zebrin II seen in transverse section reveals that subsets of Purkinje cells expressing zebrin II (*black arrow*) are interposed by similar stretches in which immunostaining is weak or absent (*white arrow*). **c** Immunostaining of a transverse section through the anterior cerebellum by using anti-zebrin II. Stripes of immunoreactive Purkinje cells are clear in the vermis. **d** Immunoperoxidase staining of a transverse section for PLCß4. Both the Purkinje cell somata and the dendrites are labeled. **e** Immunoperoxidase staining for PLCß4 in transverse section reveals that subsets of Purkinje cells expressing PLCß4 (*black arrow*) are interposed by Purkinje cells with weak or no immunostaining (*white arrow*). **f** A transverse section through the anterior cerebellum immunostained by using anti-PLCß4. Stripes of immunoreactivity are clear in the vermis. **g** Double immunofluorescence staining of a transverse section through the anterior cerebellum, for zebrin II (*green*) and CaBP (*red*). CaBP is expressed in all Purkinje cells. The gaps between the zebrin II+ stripes are filled by CaBP+/zebrin II− Purkinje cells. **h** A transverse section through the anterior cerebellum, double immunofluorescence stained for PLCß4 (*green*) and CaBP (*red*). The spaces between the PLCß4+ stripes are filled by CaBP+/PLCß4+ Purkinje cells. **i** A transverse section through the anterior cerebellum, double immunofluorescence stained for zebrin II (*green*) and PLCß4 (*red*). Stripes of zebrin II immunoreactivity are complementary to stripes of PLCß4 expression. Lobules are indicated by *Roman numerals*. *Scale bars*=50 μm in **a** (applies to **a**, **d**); 100 μm in **b**; 250 μm in **c** (applies to **c**, **f**–**g**); 100 μm in **e**; 500 μm in **h** and **I** (color figure online)

midline, and a fourth pair (P4+) is in the paravermis (Fig. 4a, c, e). Both the P1+ and P2+ stripes extend continuously throughout the anterior lobe from lobule I to lobule V (Figs. 3 and 4a, c, e). The P+ stripes are separated by broad stripes of zebrin II−/PLCß4+ Purkinje cells (P1−, P2−; Fig. 4b, d). Three substripes are apparent within P1− (e.g., lobule III; Fig. 5a–c). A substripe architecture is also being present in P2− (likely comprising a strongly immunoreactive PLCß4+ substripe medially and a weakly immunoreactive PLCß4+ substripes laterally (Fig. 5a–c). From time to time, the PLCß4+ substripes are separated by narrow, interdigitating zebrin II+ stripes but their occurrence is irregular (e.g., Fig. 5c), and in other sections, substripes seem to be separated by acellular raphes or reflected in changes in anti-PLCß4+ staining intensity, and no zebrin II+ stripes are seen: (Fig. 5a–c). The alternating pattern of zebrin II and PLCß4 expression extends into the dorsal (posterosuperior) bank of the primary fissure (arrowhead; Fig. 4c–e), where the P+ and P− stripes are clearly revealed by both anti-zebrin II and anti-PLCß4 immunocytochemistry (zebrin II, Fig. 4a, c; PLCß4, Fig. 4b, d).

CZ

In most mammals studied to date, the AZ interdigitates with the CZ within the primary fissure [36]. The CZ is identified as a uniformly zebrin II+/PLCß4− zone that occupies most of lobules VI and VII in the mouse [4, 11]. In the star-nosed mole, a uniformly zebrin II+/PLCß4− expression domain is present but is unusually small, occupying only the dorsal part of lobule VI (Fig. 6a, b). The finding that the CZ does not occupy all of VI/VII is not surprising—there are several instances in which lobulation and transverse zone boundaries are uncoupled, e.g., [37]. In caudal lobule VI and rostral lobule VII, the pattern of uniform zebrin II+/PLCß4− expression domain is replaced by the alternating stripes of the large PZ (Figs. 6a, c–g and 7).

PZ

The most prominent feature of the mammalian and avian PZ is an array of alternating broad P+/P− stripes (reviewed in [39]). In *Condylura*, the PZ is unusually large but anti-zebrin II and

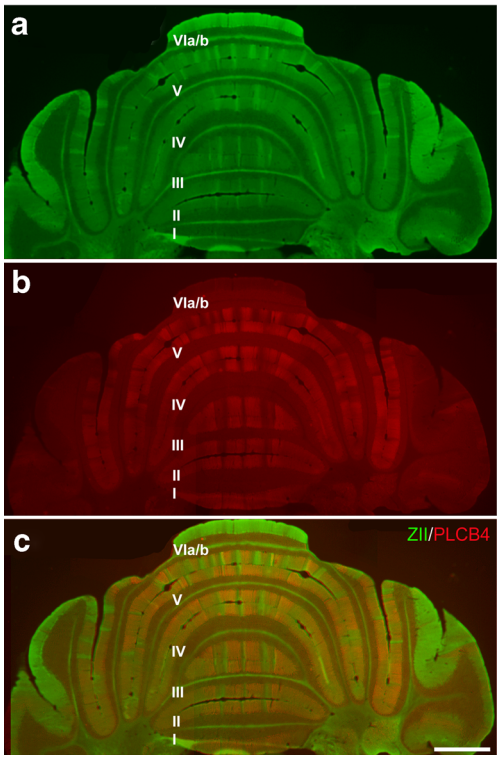

Fig. 3 Transverse section through the anterior cerebellum of the star-nosed mole, double immunostained for zebrin II (*green*, **a**) and PLCß4 (*red*, **b**; *merged*, **c**). Lobules in the vermis are indicated by *Roman numerals*. *Scale bars*=1 mm (color figure online)

anti-PLCß4 immunocytochemistry nonetheless reveal a characteristic array of alternating stripes that extend continuously from lobule VII to IX (Figs. 6a and 7a–c, f–h).

NZ

In most mammals, the NZ is a uniformly zebrin II+/PLCß4− zone that occupies lobule X and interdigitates with the PZ in lobule IX. In the star-nosed mole, lobules IX (Fig. 7d–e) and X (Fig. 7i) are predominantly zebrin II+ but stripes can still be discerned through lobule IXb (Fig. 7d, i).

Hemispheres

The striped architecture of the vermis extends into the hemispheres, and the typical mammalian distribution is generally present, although again with exceptions. The striped array seen in the vermis of lobules VI–VII extends laterally into the putative simplex and ansiform lobules (Fig. 3a–c). First, in most mammals, lobulus simplex a is striped whereas lobulus simplex b is uniformly zebrin II+. In the star-nosed mole, the patterns of zebrin II (Fig. 8a) and PLCß4 (Fig. 8b) expression in the lobulus simplex are striped and complementary (Fig. 8c). However, no uniformly zebrin II+/PLCß4−

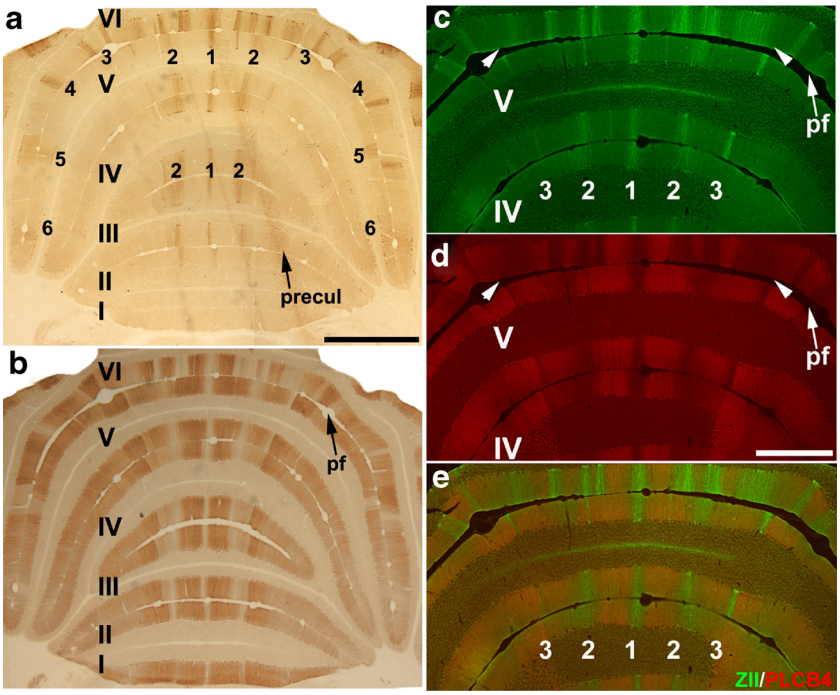

Fig. 4 The AZ of the cerebellar vermis of the star-nosed mole. **a** A transverse section through the lobules I–V immunoperoxidase stained by using anti-zebrin II. Narrow stripes of zebrin II+ Purkinje cells are present in the AZ. The P1+ to P4+ stripes in lobules II–V are labeled (as *1–4*). **b** A serial transverse section through the lobules I–V immunoperoxidase stained by using anti-PLCß4. Broad stripes of PLCß4+ Purkinje cells are separated by narrow stripes of PLCß4− Purkinje cells. **c**, **d** Double immunofluorescence staining for zebrin II (*green*) and PLCß4 (*red*) of a transverse section through lobules IV–V of the vermis. Stripes of zebrin II+ and PLCß4+ Purkinje cells are complementary. *Precul* preculminate fissure, *pf* primary fissure. *Scale bars*=1 mm in **a** (applies to **a**, **b**); 500 μm in **d** (applies in **c**–**e**) (color figure online)

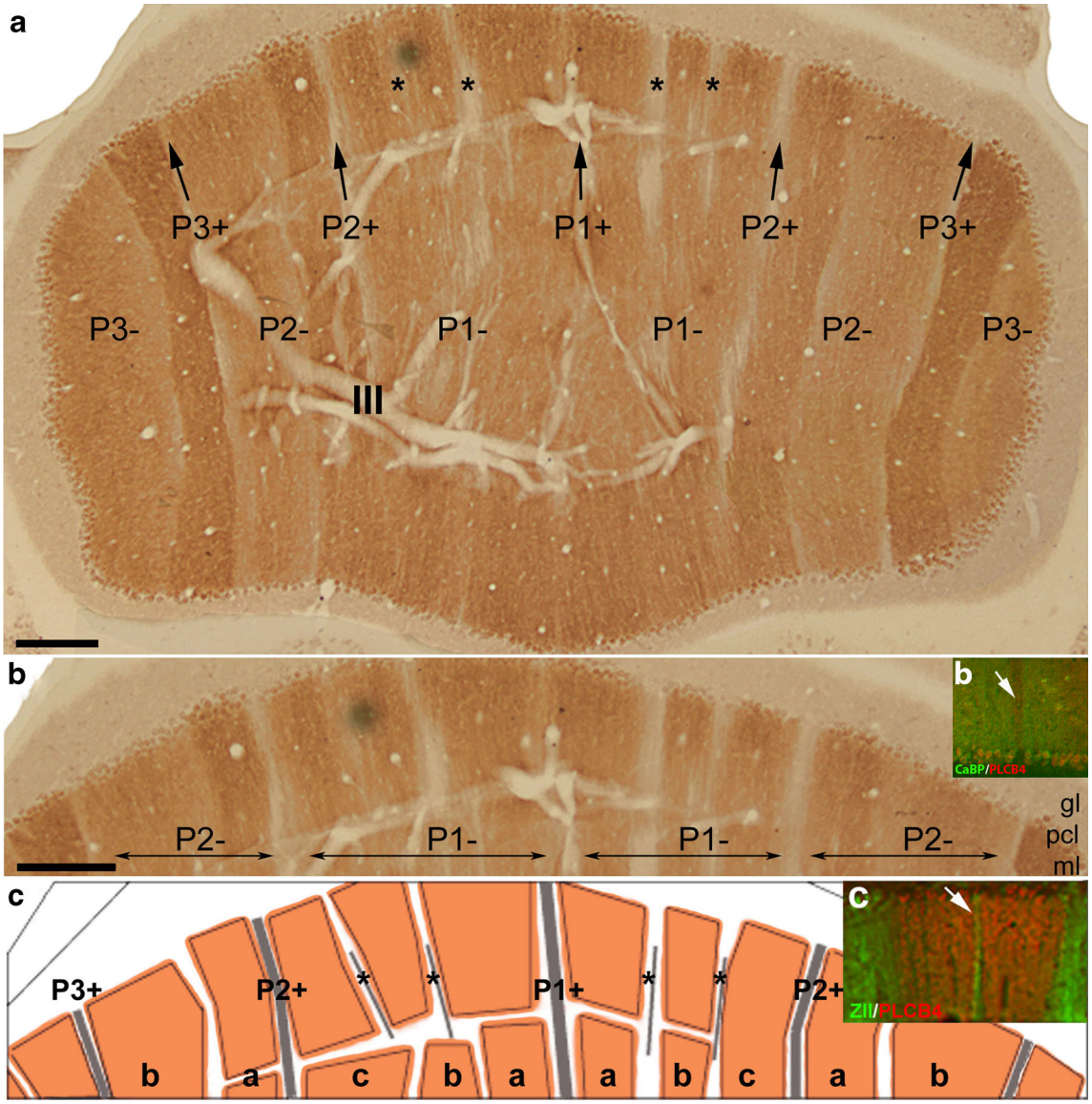

Fig. 5 **a**–**c** Transverse sections through the vermis of lobule III, immunoperoxidase stained for PLCß4 show substripes within P1− and P2−. A high magnification view is shown in **b** and summarized in cartoon form in **c**. Within P1−, three PLCß4+ stripes are separated by two narrow stripes of zebrin II+ Purkinje cells (*asterisks*). *Inset* in **b** indicates an acellular raphe/space. *Inset* in **c** shows zebrin II+ Purkinje cells within the PLCß4+ stripes. *Scale bars*=250 μm in **a** and **b**

lobulus simplex b is apparent. Secondly, in most mammals, the ansiform lobule is divided by the intracrural fissure into crus I and crus II, and both reveal a well-defined pattern of zebrin II/PLCß4 stripes (e.g., [11, 14]). The same is the case in the star-nosed mole: crus I and crus II are very large with prominent fissures that further subdivide them into crus Ia/b and crus IIa/b (Fig. 1a). In both crus I and crus II, zebrin II+ and PLCß4+ Purkinje cells form an alternating stripe array (Fig. 8d, e) that extends to the paraflocculus (Fig. 8d, e). In the star-nosed mole, all Purkinje cells appear to be zebrin II+ in the flocculus, as is the case in many other mammals (data not shown).

Discussion

General Anatomy

Despite differences in the gross anatomy of the cerebellum between mouse and star-nosed mole (such as the large vermis with elongated lobule VI/VII and relatively small lobule VIII) we have numbered cerebellar lobules in the star-nosed mole in a way we believe to be consistent with the schemata adopted in rodents (e.g., [55]). The three principal fissures—the primary fissure, prepyramidal fissure, and posterolateral fissure—are conserved across the Mammalia and are reliably identified in the star-nosed mole, and despite the small lobule

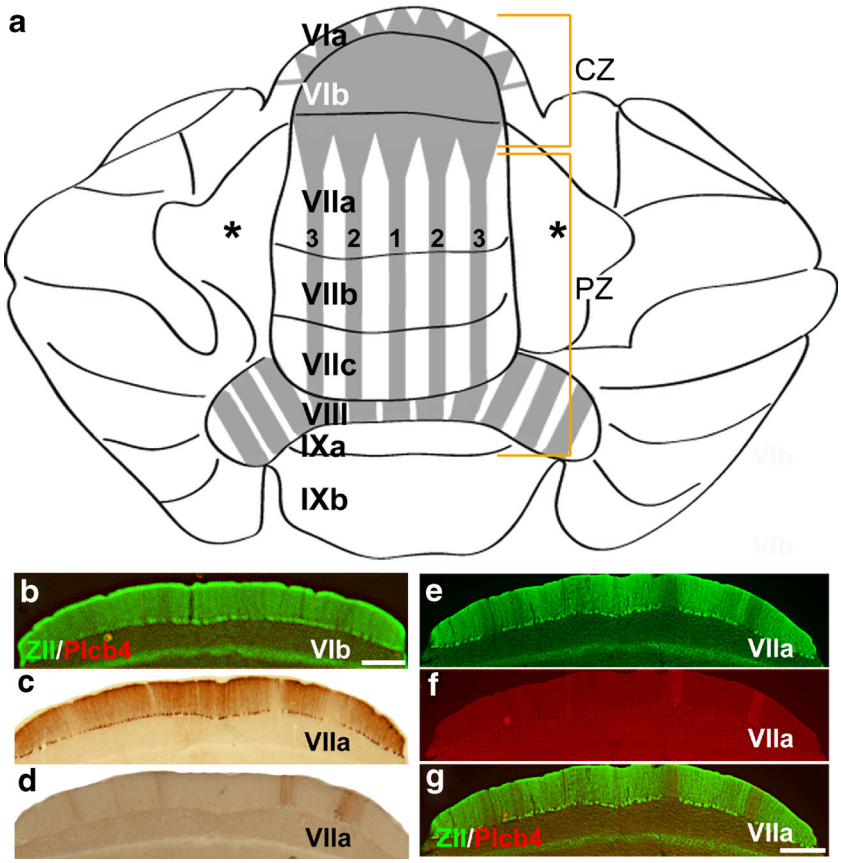

Fig. 6 The CZ of the star-nosed mole. **a** A cartoon of the dorsal aspect of the star-nosed mole cerebellum indicating the pattern of zebrin II and PLCß4 expression in the CZ and PZ (the P1+ to P3+ stripes of the PZ are labeled as *1*, *2*, and *3*). **b** Double immunofluorescence staining of a transverse section through the lobules VIb for zebrin II (*green*) and PLCß4 (*red*). The uniform pattern of zebrin II expression in lobule VIb (= CZ) is accompanied by a lack of PLCß4 expression. **c**, **d** Transverse serial sections through lobule VIIa immunoperoxidase-stained for zebrin II (**c**) and PLCß4 (**d**). Almost all Purkinje cells are zebrin II/PLCß4−. **e**–**g** Double immunofluorescence staining of a transverse section through the anterior part of lobule VIIa for zebrin II (*green*) and PLCß4 (*red*) and merged in **g**. Almost all Purkinje cells are zebrin II/PLCß4 −. *Scale bars*=250 μm in **b**; 250 μm in **g** (applies to **c**–**g**) (color figure online)

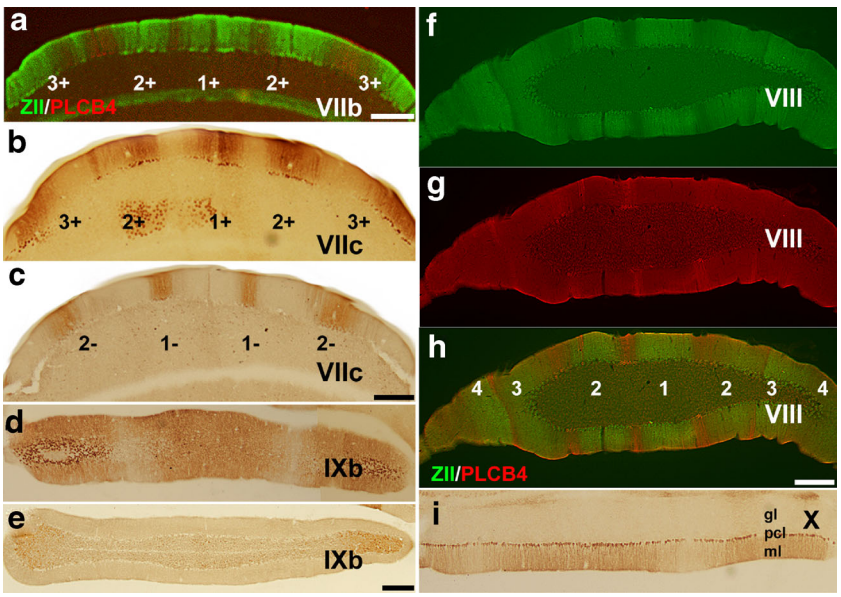

Fig. 7 The PZ and NZ of the cerebellum of the star-nosed mole. **a** Double immunofluorescence staining of a transverse section through lobules VIIb for zebrin II (*green*) and PLCß4 (*red*). **b**, **c** Transverse serial sections through the lobule VIIc immunoperoxidase-stained for zebrin II (**b**) and PLCß4 (**c**). Zebrin II and PLCß4 are expressed in complementary stripes. **d**, **e** Transverse serial sections through the lobules IX immunoperoxidase-stained for zebrin II (**d**) and PLCß4 (**e**). **f**–**h** Double immunofluorescence staining of a transverse section through the lobule VIII for zebrin II (*green*) and PLCß4 (*red*): the stripe patterns are complementary. **i** A transverse section through the lobules X immunoperoxidase-stained for zebrin II shows a uniform expression profile. *gl* granular layer, *pcl* Purkinje cell layer, *ml* molecular layer. *Scale bars*=250 μm in **a**; 250 μm in **c** (applies to **b**, **c**, **i**); 250 μm in **e** (applies to **d**–**e**); 250 μm in **h** (applies to **f**–**h**) (color figure online)

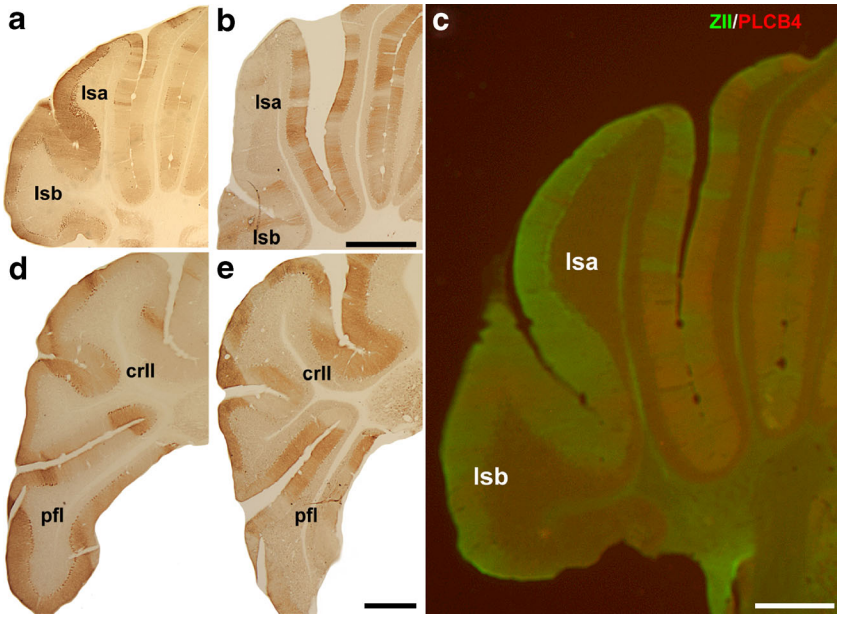

Fig. 8 The striped architecture in the hemispheres of the star-nosed mole cerebellum. **a**, **b** Serial transverse sections immunocytochemically stained for zebrin II (**a**) and PLCß4 (**b**) reveal a striped architecture in the hemispheres: the stripe sets are complementary. **c** Double immunofluorescence staining of a transverse section through the hemisphere for zebrin II (*green*) and PLCß4 (*red*). The stripe patterns are complementary. **d**, **e** Serial transverse sections through the paraflocculus (pfl) immunoperoxidase stained for zebrin II (**d**) and PLCß4 (**e**). *lsa* lobulus simplex a, *lsb* lobulus simplex b, *crII* crus II. *Scale bars*=1 mm in **b** (applies to **a**, **b**); 500 μm in **e** (applies to **d**, **e**); 500 μm in **c** (color figure online)

VIII, the prepyramidal and secondary fissures are still distinguishable in sagittal sections (Fig. 1).

The zone-and-stripe architecture of the cerebellum generally conforms to the pattern reported from many species in the past (e.g., [38, 39]) but also has three specific features worthy of note:

1. Substripes within the P1−/P2− stripes of the AZ*:* Similar substripes have been reported during mouse development, where three distinct PLCß4+ clusters fuse in the first postnatal week to form a single stripe [12]. This triplet structure of P1−/P2− is also reflected in the segregation of spinocerebellar and cuneocerebellar mossy fiber terminal fields (e.g., [17]) and in the expression of an L7/pcp2-*lacZ* transgene [4]. However, the presence of narrow intervening zebrin II+ stripes separating the subzones (Figs. 4c and 5a) has not been seen before. These stripes may be related to the so-called "satellite" stripes irregularly seen in rodents (e.g., [56]).
2. Small CZ: In mice, the CZ occupies lobules VI and VII. However, in the star-nosed mole, it is much smaller and restricted to lobule VI (and even then is not evident in the more ventral part; Figs. 4a, b and 9). Whether both a CZa and a CZp is present despite the small size cannot be determined as specific markers for CZ subzones in mouse (HSP25 [32]; neurofilament-associated antigen [31]) were not detected in the star-nosed mole. The evolutionary explanation for a small CZ may lie in the fact that star-nosed moles are blind. The CZ is a prominent cerebellar visual-receiving area (e.g., [57, 58]). In Fig. 9, the vermis of the star-nosed mole is compared to that of the mouse and another visually impaired species, the naked mole-rat [36]. In both cases, the CZ is much smaller than in the mouse. Therefore, it is plausible to speculate that the proportionally small CZ reflects the lack of visual input. This may also explain why the NZ in the star-nosed mole is proportionally small compared to mouse but comparable to that in the naked mole-rat (Fig. 9). It should be emphasized that this is an evolved feature: for example, the surgical removal of visual input in a newborn mouse has no effect on the size or stripe architecture of the CZ [59].
3. Relative expansion of the PZ, crus I, and crus II: The most striking sensory feature of *Condylura* is the "star," a highly sensitive mechanosensory adaptation of the trigeminal system [45, 60]. In mammals, sensory information from the face, snout and vibrissa and rays is carried by the trigeminal nerve. Consistent with the prominent role of the somatosensory system in the star-nosed mole, the somatosensory map in the primary sensory cortex resembles a visual system map rather than a typical barrel cortex with receptive input from vibrissae. Furthermore, not only do tactile fovea in the star-nosed mole function similarly to the retinal fovea in other mammals, they are also comparable with the acoustic fovea of bats [46]. Trigeminocerebellar mossy fibers terminate in the AZ

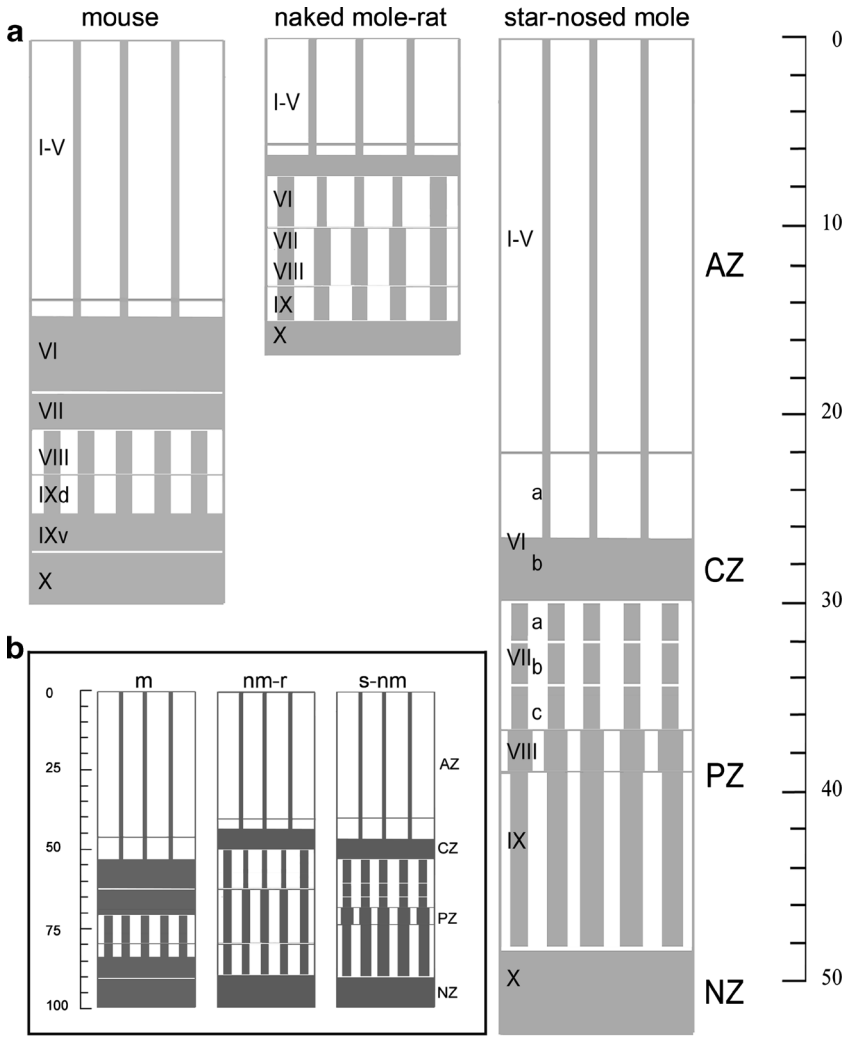

Fig. 9 Unfolded representations of the vermis of the mouse (m), naked mole-rat (nm-r; [36]), and star-nosed mole (s-nm) cerebella compared for the pattern of zebrin II expression. **a** The three unfolded cerebella are shown to scale (mm). Uniform zebrin II expression is indicated by *solid boxes* and striped expression by *lines*. Compared to the mouse, the visual receiving areas (the CZ and NZ) are reduced in relative size in the two blind species (naked mole-rat and star-nosed mole) and the trigeminal-receiving PZ in the star-nosed mole is relatively enlarged, possibly reflecting the enhanced importance of the trigeminal system. The PZ extends from rostral lobule VII to caudal lobule IX in the star-nosed mole, and leaves the small CZ to occupy only the dorsal portion of lobule VIb. The NZ is restricted to lobule X. **b** The three unfolded cerebella are redrawn to the same length to emphasize the proportional differences in size between transverse zones

and PZ, in register with the zebrin II+/− stripes [22, 35, 61–63]. There are also prominent trigeminocerebellar inputs to the hemispheres especially to the crus II region of the cerebellum [64–67]. Consistent with the importance of the star appendages, all three areas in the star-nosed mole are prominent (AZ, Fig. 4; PZ, Fig. 7; hemispheres, Fig. 8). For example, Fig. 9 shows that the PZ of the vermis is relatively enlarged compared to the mouse, consistent with the hypothesis that PZ expansion correlates with the expanded role of trigeminal inputs. Finally, the NZ is proportionally rather small, which is also the case in the naked mole-rat (Fig. 9b). The NZ, like the CZ, receives prominent inputs from the visual system (e.g., [68]), and so the small size may reflect both species are blind.

An extreme example of an unusual mammalian lifestyle is found in the bats. We recently described the zone-and-stripe architecture in several species of microchiropteran bat [41]. While the overall architecture of the bat cerebellum resembles that in other mammals, the transverse zonation has two novel features. First, an additional transverse zone is found in lobule I (= lingular zone, [41]), a feature previously only encountered in the avian cerebellum [33–35]. Secondly, the CZ in bats is elaborated from two zones to four, two uniformly zebrin II+/PLCß4− and two striped. Two hypotheses can be advanced to explain the unusual transverse zone architecture in bats—either that it reflects an adaptation to flight and/or to echolocation [41] or it is an evolved characteristic of the clade independent of the special adaptations. Surprisingly, the talpids are phylogenetically part of a monophyletic group with the bats and are more closely related to bats than they are to mole-rats or tenrecs (e.g., [69]; albeit that the last common ancestor of bats and talpids likely lived about 65–75 million years ago, so there has been much time for divergent evolution to have taken place in both lineages). There is no evidence of either a lingular zone or an elaborated CZ in *Condylura*, consistent with the hypothesis that these features evolved to subserve flight and echolocation, respectively, and are not shared characteristics of the clade. It will be interesting to see if similar adaptations are found in the Macrochiroptera.

In conclusion, the zone-and-stripe architecture of the mammalian cerebellum has been analyzed in more than 20 species and generally, it has been the similarities between species rather than the differences that have drawn attention (e.g., [38, 39]). However, species-specific cerebellar characteristics are also present (e.g., an LZ in birds [33–35], an LZ and expanded CZ in bats [41], and an enlarged PZ in the naked mole-rat [36]). In the case of the star-nosed mole, the unusual features of cerebellar architecture, such as the small CZ and large PZ, can plausibly be correlated with adaptations to blindness and enlarged trigeminocerebellar input from the star. These findings are not consistent with a model in which all cerebellar regions adapt in concert but rather point to a mosaic structure with distinct regions—in these cases, transverse zones—upon which selection pressure acts, in part, independently.

This and other comparative studies of cerebellar compartmentation raise the general issue of whether the cerebellum is a collection independently varying modules (zones and stripes) or should be treated as a single entity. Examples of regional (allometric) brain adaptations have often been mapped in the cortex. For example, enlarged forelimb tactile representations in the cortices of primates, raccoons [70], and moles [71]. In addition, naked mole rats have a huge cortical representation of the front teeth and reduced cortical visual representations (e.g., the naked mole-rat [72]). These and other examples suggest the hypothesis that increase or decrease in relative size of a brain region is driven by functional augmentation [70]. While the sample is small, the same may apply in the cerebellum, for example, the reduced CZ in the blind naked mole-rat [36] and the enhanced trigeminal receiving areas in the star-nosed mole (e.g., Fig. 9). This suggests that a version of allometric scaling may apply within the cerebellum as well as to the elaboration of the cerebellum as a whole (e.g., [73]). By the cerebellar allometry hypothesis, individual transverse zones in the cerebellum can independently expand or reduce in relative size sensory inputs evolve, while still retaining their characteristic mammalian striped architecture [Bats may be an exception: novel or atypical adaptation of lobule I ("lingular zone") and hypertrophy and atypical architecture of the CZ (lobules VI/VII)]. Presumably, transverse zone size is determined early in development by altering the number of Purkinje cells destined to give rise to the zone. In turn, this implies that different parts of the cerebellar anlage in the fourth ventricle are fated to generate different zones (consistent with the birth dating restriction evidence, e.g., [74] and reviewed in [5]).

Acknowledgments These studies were supported by grants from the Canadian Institutes of Health Research (RH), the Manitoba Health Research Council (HM), and the NIH (DE016061: KCC) and NSF (0844743: KCC). We thank Dr. Kevin Campbell (U. Manitoba) for advice on phylogeny.

Conflict of Interest The authors have no conflict of interest.

References

1. Hawkes RBG, Doré L, Gravel C, Leclerc N. Zebrins: molecular markers of compartmentation in the cerebellum. In: Llinás RSC, editor. The cerebellum revisited. New York: Springer; 1992. p. 22–55.
2. Hawkes R. An anatomical model of cerebellar modules. Prog Brain Res. 1997;114:39–52.
3. Herrup K, Kuemerle B. The compartmentalization of the cerebellum. Annu Rev Neurosci. 1997;20:61–90.
4. Ozol K, Hayden JM, Oberdick J, Hawkes R. Transverse zones in the vermis of the mouse cerebellum. J Comp Neurol. 1999;412:95–111.
5. Apps R, Hawkes R. Cerebellar cortical organization: a one-map hypothesis. Nat Rev Neurosci. 2009;10:670–81.
6. Armstrong CL, Hawkes R. Pattern formation in the cerebellar cortex. Biochem. Cell Biol. 2000;78:551–562.
7. Brochu G, Maler L, Hawkes R. Zebrin II: a polypeptide antigen expressed selectively by Purkinje cells reveals compartments in rat and fish cerebellum. J Comp Neurol. 1990;291:538–52.
8. Hawkes R, Gravel C. The modular cerebellum. Prog Neurobiol. 1991;36:309–27.
9. Ahn AH, Dziennis S, Hawkes R, Herrup K. The cloning of zebrin II reveals its identity with aldolase C. Development. 1994;120:2081–90.
10. Hawkes R, Herrup K. Aldolase C/zebrin II and the regionalization of the cerebellum. J Mol Neurosci. 1995;6:147–58.
11. Sarna JR, Marzban H, Watanabe M, Hawkes R. Complementary stripes of phospholipase Cbeta3 and Cbeta4 expression by Purkinje cell subsets in the mouse cerebellum. J Comp Neurol. 2006;496:303–13.
12. Marzban H, Chung S, Watanabe M, Hawkes R. Phospholipase Cbeta4 expression reveals the continuity of cerebellar topography through development. J Comp Neurol. 2007;502:857–71.
13. Eisenman LM, Hawkes R. Antigenic compartmentation in the mouse cerebellar cortex: zebrin and HNK-1 reveal a complex, overlapping molecular topography. J Comp Neurol. 1993;335:586–605.
14. Sillitoe RV, Hawkes R. Whole-mount immunohistochemistry: a high-throughput screen for patterning defects in the mouse cerebellum. J Histochem Cytochem. 2002;50:235–44.
15. Gravel C, Hawkes R. Parasagittal organization of the rat cerebellar cortex: direct comparison of Purkinje cell compartments and the organization of the spinocerebellar projection. J Comp Neurol. 1990;291:79–102.
16. Akintunde A, Eisenman LM. External cuneocerebellar projection and Purkinje cell zebrin II bands: a direct comparison of parasagittal banding in the mouse cerebellum. J Chem Neuroanat. 1994;7:75–86.
17. Ji Z, Hawkes R. Topography of Purkinje cell compartments and mossy fiber terminal fields in lobules II and III of the rat cerebellar cortex: spinocerebellar and cuneocerebellar projections. Neuroscience. 1994;61:935–54.
18. Ruigrok TJ. Ins and outs of cerebellar modules. Cerebellum. 2010;10:464–74.
19. Gravel C, Eisenman LM, Sasseville R, Hawkes R. Parasagittal organization of the rat cerebellar cortex: direct correlation between antigenic Purkinje cell bands revealed by mabQ113 and the organization of the olivocerebellar projection. J Comp Neurol. 1987;265:294–310.
20. Voogd J, Pardoe J, Ruigrok TJ, Apps R. The distribution of climbing and mossy fiber collateral branches from the copula pyramidis and the paramedian lobule: congruence of climbing fiber cortical zones and the pattern of zebrin banding within the rat cerebellum. J Neurosci. 2003;23:4645–56.

21. Sugihara I, Shinoda Y. Molecular, topographic, and functional organization of the cerebellar cortex: a study with combined aldolase C and olivocerebellar labeling. J Neurosci. 2004;24:8771–85.
22. Chockkan V, Hawkes R. Functional and antigenic maps in the rat cerebellum: zebrin compartmentation and vibrissal receptive fields in lobule IXa. J Comp Neurol. 1994;345:33–45.
23. Chen G, Hanson CL, Ebner TJ. Functional parasagittal compartments in the rat cerebellar cortex: an in vivo optical imaging study using neutral red. J Neurophysiol. 1996;76:4169–74.
24. Hallem JS, Thompson JH, Gundappa-Sulur G, Hawkes R, Bjaalie JG, Bower JM. Spatial correspondence between tactile projection patterns and the distribution of the antigenic Purkinje cell markers anti-zebrin I and anti-zebrin II in the cerebellar folium crus IIA of the rat. Neuroscience. 1999;93:1083–94.
25. Wadiche JI, Jahr CE. Patterned expression of Purkinje cell glutamate transporters controls synaptic plasticity. Nat Neurosci. 2005;8:1329–34.
26. Horn KM, Pong M, Gibson AR. Functional relations of cerebellar modules of the cat. J Neurosci. 2010;30:9411–23.
27. Paukert M, Huang YH, Tanaka K, Rothstein JD, Bergles DE. Zones of enhanced glutamate release from climbing fibers in the mammalian cerebellum. J Neurosci. 2010;30:7290–9.
28. Zhou H, Lin Z, Voges K, Ju C, Gao Z, Bosman LW, et al. Cerebellar modules operate at different frequencies. eLife. 2014;3:e02536.
29. Graham DJ, Wylie DR. Zebrin-immunopositive and -immunonegative stripe pairs represent functional units in the pigeon vestibulocerebellum. J Neurosci. 2012;32:12769–79.
30. Xiao J, Cerminara NL, Kotsurovskyy Y, Aoki H, Burroughs A, Wise AK, et al. Systematic regional variations in Purkinje cell spiking patterns. PLoS One. 2014;9:e105633.
31. Marzban H, Kim CT, Doorn D, Chung SH, Hawkes R. A novel transverse expression domain in the mouse cerebellum revealed by a neurofilament-associated antigen. Neuroscience. 2008;153:1190–201.
32. Armstrong CL, Krueger-Naug AM, Currie RW, Hawkes R. Constitutive expression of the 25-kDa heat shock protein Hsp25 reveals novel parasagittal bands of purkinje cells in the adult mouse cerebellar cortex. J Comp Neurol. 2000;416:383–97.
33. Pakan JM, Iwaniuk AN, Wylie DR, Hawkes R, Marzban H. Purkinje cell compartmentation as revealed by zebrin II expression in the cerebellar cortex of pigeons (*Columba livia*). J Comp Neurol. 2007;501:619–30.
34. Iwaniuk AN, Marzban H, Pakan JM, Watanabe M, Hawkes R, Wylie DR. Compartmentation of the cerebellar cortex of hummingbirds (Aves: Trochilidae) revealed by the expression of zebrin II and phospholipase C beta 4. J Chem Neuroanat. 2009;37:55–63.
35. Marzban H, Chung SH, Pezhouh MK, Feirabend H, Watanabe M, Voogd J, et al. Antigenic compartmentation of the cerebellar cortex in the chicken (*Gallus domesticus*). J Comp Neurol. 2010;518:2221–39.
36. Marzban H, Hoy N, Aavani T, Sarko DK, Catania KC, Hawkes R. Compartmentation of the cerebellar cortex in the naked mole-rat (*Heterocephalus glaber*). Cerebellum. 2011;10:435–48.
37. Beierbach E, Park C, Ackerman SL, Goldowitz D, Hawkes R. Abnormal dispersion of a purkinje cell subset in the mouse mutant cerebellar deficient folia (cdf). J Comp Neurol. 2001;436:42–51.
38. Sillitoe RV, Marzban H, Larouche M, Zahedi S, Affanni J, Hawkes R. Conservation of the architecture of the anterior lobe vermis of the cerebellum across mammalian species. Prog Brain Res. 2005;148:283–97.
39. Marzban H, Hawkes R. On the architecture of the posterior zone of the cerebellum. Cerebellum. 2010;10:422–34.
40. Meek J, Hafmans TG, Maler L, Hawkes R. Distribution of zebrin II in the gigantocerebellum of the mormyrid fish Gnathonemus petersii compared with other teleosts. J Comp Neurol. 1992;316:17–31.
41. Kim JY, Marzban H, Chung SH, Watanabe M, Eisenman LM, Hawkes R. Purkinje cell compartmentation of the cerebellum of microchiropteran bats. J Comp Neurol. 2009;517:193–209.
42. Finlay BL, Darlington RB. Linked regularities in the development and evolution of mammalian brains. Science. 1995;268:1578–84.
43. de Winter W, Oxnard CE. Evolutionary radiations and convergences in the structural organization of mammalian brains. Nature. 2001;409:710–4.
44. Catania KC. A nose that looks like a hand and acts like an eye: the unusual mechanosensory system of the star-nosed mole. J Comp Physiol A. 1999;185:367–72.
45. Gerhold KA, Pellegrino M, Tsunozaki M, Morita T, Leitch DB, Tsuruda PR, et al. The star-nosed mole reveals clues to the molecular basis of mammalian touch. PLoS One. 2013;8:e55001.
46. Catania KC. The sense of touch in the star-nosed mole: from mechanoreceptors to the brain. Phil Trans Roy Soc Lond Series B. 2011;366:3016–25.
47. Walther EU, Dichgans M, Maricich SM, Romito RR, Yang F, Dziennis S, et al. Genomic sequences of aldolase C (Zebrin II) direct lacZ expression exclusively in non-neuronal cells of transgenic mice. Proc Natl Acad Sci U S A. 1998;95:2615–20.
48. Nakamura M, Sato K, Fukaya M, Araishi K, Aiba A, Kano M, et al. Signaling complex formation of phospholipase Cbeta4 with metabotropic glutamate receptor type 1alpha and 1,4,5-trisphosphate receptor at the perisynapse and endoplasmic reticulum in the mouse brain. Eur J Neurosci. 2004;20:2929–44.
49. Baimbridge KG, Miller JJ. Immunohistochemical localization of calcium-binding protein in the cerebellum, hippocampal formation and olfactory bulb of the rat. Brain Res. 1982;245:223–9.
50. Marzban H, Hawkes R. Fibroblast growth factor promotes the development of deep cerebellar nuclear neurons in dissociated mouse cerebellar cultures. Brain Res. 2007;1141:25–36.
51. Marzban H, Sillitoe RV, Hoy M, Chung SH, Rafuse VF, Hawkes R. Abnormal HNK-1 expression in the cerebellum of an N-CAM null mouse. J Neurocytol. 2004;33:117–30.
52. Voogd J. Cerebellum. In: Paxinos G, editor. The Rat Nervous System. 2nd ed. San Diego: Academic Press Inc; 1995. p. 309–50.
53. Sanchez M, Sillitoe RV, Attwell PJ, Ivarsson M, Rahman S, Yeo CH, et al. Compartmentation of the rabbit cerebellar cortex. J Comp Neurol. 2002;444:159–73.
54. Marzban H, Zahedi S, Sanchez M, Hawkes R. Antigenic compartmentation of the cerebellar cortex in the syrian hamster Mesocricetus auratus. Brain Res. 2003;974:176–83.
55. Larsell O. The Comparative Anatomy and Histology of the Cerebellum from Monotremes through Apes. Minneapolis: University of Minnesota Press; 1970. p. 269.
56. Hawkes R, Leclerc N. Immunocytochemical demonstration of topographic ordering of Purkinje cell axon terminals in the fastigial nuclei of the rat. J Comp Neurol. 1986;244:481–91.
57. Voogd J, Barmack NH. Oculomotor cerebellum. Prog Brain Res. 2006;151:231–68.
58. Kralj-Hans I, Baizer JS, Swales C, Glickstein M. Independent roles for the dorsal paraflocculus and vermal lobule VII of the cerebellum in visuomotor coordination. Exp Brain Res. 2007;177:209–22.
59. Armstrong CL, Krueger-Naug AM, Currie RW, Hawkes R. Expression of heat-shock protein Hsp25 in mouse Purkinje cells during development reveals novel features of cerebellar compartmentation. J Comp Neurol. 2001;429:7–21.
60. Catania KC. Epidermal sensory organs of moles, shrew moles, and desmans: a study of the family talpidae with comments on the function and evolution of Eimer's organ. Brain Behav Evol. 2000;56:146–74.
61. Somana R, Kotchabhakdi N, Walberg F. Cerebellar afferents from the trigeminal sensory nuclei in the cat. Exp Brain Res. 1980;38:57–64.
62. Voogd J, Gerrits NM, Ruigrok TJ. Organization of the vestibulocerebellum. Ann NY Acad Sci. 1996;781:553–79.
63. Voogd J, Ruigrok TJ. Transverse and longitudinal patterns in the mammalian cerebellum. Prog Brain Res. 1997;114:21–37.

64. Saigal RP, Karamanlidis AN, Voogd J, Mangana O, Michaloudi H. Secondary trigeminocerebellar projections in sheep studied with the horseradish peroxidase tracing method. J Comp Neurol. 1980;189: 537–53.
65. Falls WM. Direct connections of primary trigeminal afferent axons with trigeminocerebellar projection neurons in the border zone of rat trigeminal nucleus oralis. Neurosci Lett. 1987;83:247–52.
66. Falls WM, Alban MM. Morphological features of identified trigeminocerebellar projection neurons in the border zone of rat trigeminal nucleus oralis. Somatosens Res. 1986;4:1–12.
67. Brown IE, Bower JM. The influence of somatosensory cortex on climbing fiber responses in the lateral hemispheres of the rat cerebellum after peripheral tactile stimulation. J Neurosci. 2002;22:6819–29.
68. Voogd J, Schraa-Tam CK, van der Geest JN, De Zeeuw CI. Visuomotor cerebellum in human and nonhuman primates. Cerebellum. 2012;11:392–410.
69. Meredith RW, Janecka JE, Gatesy J, Ryder OA, Fisher CA, Teeling EC, et al. Impacts of the cretaceous terrestrial revolution and KPg extinction on mammal diversification. Science. 2011;334:521–4.
70. Deacon TW. The evolution of language systems in the human brain. In: Kaas JH, editor. Evolution of nervous systems. 4. London: Elsevier; 2007. p. 529–47.
71. Catania KC, Kaas JH. Organization of somatosensory cortex and distribution of corticospinal neurons in the eastern mole (Scalopus aquaticus). J Comp Neurol. 1997;378:337–53.
72. Catania KC, Remple MS. Somatosensory cortex dominated by the representation of teeth in the naked mole-rat brain. Proc Natl Acad Sci U S A. 2002;99:5692–7.
73. Yopak KE, Lisney TJ, Darlington RB, Collin SP, Montgomery JC, Finlay BL. A conserved pattern of brain scaling from sharks to primates. Proc Natl Acad Sci U S A. 2010;107:12946–51.
74. Hashimoto M, Mikoshiba K. Mediolateral compartmentalization of the cerebellum is determined on the "birth date" of Purkinje cells. J Neurosci. 2003;23:11342–51.